ACTA CHEMICA SCANDINAVICA 26 (1972) 719–732

Equiatomic Transition Metal Alloys of Manganese

VIII. Structural and Magnetic Properties of Rh – Mn Phases

KARI SELTE,[a] E. BJERKELUND,[a] A. KJEKSHUS,[a] A. F. ANDRESEN,[b] W. B. PEARSON[c] and V. MEISALO[d]

[a]*Kjemisk Institutt, Universitetet i Oslo, Blindern, Oslo 3, Norway,* [b]*Institutt for Atomenergi, Kjeller, Norway,* [c]*Department of Physics, University of Waterloo, Waterloo, Ontario, Canada, and* [d]*Department of Physics, University of Helsinki, Helsinki 17, Finland*

The structural and magnetic properties of well characterized Rh – Mn alloys have been studied in the range from 44 to 72 atomic % Mn. The cubic RhMn phase with CsCl type structure is stable at higher temperatures, its homogeneity range extending from 50.0 ± 0.5 to ~ 58 atomic % Mn for alloys quenched from temperatures between 500 and 950°C. Both X-ray and magnetic susceptibility measurements indicate a transition between the chemically ordered CsCl type structure for RhMn and a disordered cubic structure at temperatures between 580 and 840 K, depending on composition. The spin quantum number of Mn in chemically ordered, equiatomic cubic RhMn is $2S_{Mn} = 3.7 \pm 0.5$ ("spin only" approximation) and this parameter decreases rapidly when the Mn content exceeds 50 atomic %. The spin quantum number of Mn in the chemically disordered cubic RhMn phase shows less variation. The magnetic susceptibility data for cubic RhMn suggest that at least two different exchange mechanisms are operative. The cubic RhMn phase has not been obtained in an ordered magnetic state, paramagnetism being observed throughout its existence range.

The cubic RhMn phase transforms on cooling to a tetragonal RhMn phase with a CuAu(I) type structure. Its homogeneity range extends from ~ 53 to 68.0 ± 0.5 atomic % Mn in the room temperature region, where this phase is partly metastable. Tetragonal RhMn is in an antiferromagnetically ordered state, the direction of the moments always being perpendicular to [001]. $2S_{Mn} = 3.4 \pm 0.2$ and $2S_{Rh} < 0.2$ were found by neutron diffraction for $Rh_{45}Mn_{55}$, $2S_{Mn}$ decreasing slightly as the Mn content increases.

A simple model to account for the value of $2S_{Mn}$ as a function of structure and composition, which has previously been considered in relation to the corresponding NiMn, PdMn, PtMn, and IrMn phases, is discussed.

The ordered CsCl (cubic) and CuAu(I) (tetragonal) type crystal structures are both found in the equiatomic region of the Rh – Mn system, and although the relevant portion of the equilibrium diagram is virtually unknown

(*cf.* Hansen [1]) the cubic RhMn phase generally appears to occur at higher temperatures than the tetragonal RhMn phase.[2–5] Nakayama and Asanuma [4] have reported that the transformation between the two phases is associated with a hysteresis of about 150°C in the temperature range from −100 to 400°C according to composition.

The purpose of the present study, which forms a continuation of our examinations [6–12] of equiatomic transition metal alloys of manganese, is to elucidate the structural and magnetic properties of the cubic and tetragonal RhMn phases. For this reason we have been concerned with the preparation and measurement of well characterized alloys, rather than in establishing details of the equilibrium diagram. Nevertheless, our data also shed some light on the latter problem.

In the tetragonal NiMn, PdMn, and PtMn phases, which we have studied previously,[6,8–11] the dominant magnetic exchange interaction is between Mn atoms in the basal plane of the CuAu(I) type structure. The relatively simple magnetic situation in these phases has led us to propose a tentative model for their bonding and the magnetic exchange interactions.[9–11] The model clearly requires further testing, and the isostructural RhMn and IrMn phases (with one less valence electron per formula unit) conveniently allow this. Although we have already examined the IrMn phase,[7,12] we have not progressed far with analysis of the magnetic exchange interactions, since the alloys were still found to be in the antiferromagnetic state at temperatures up to ~1150 K. It was our hope that the analyses of the RhMn data would allow a more extensive discussion.

EXPERIMENTAL

The alloys were prepared from 99.9+% pure Rh (Johnson, Matthey & Co.) and electrolytic 99.9+% pure Mn (Johnson, Matthey & Co.; H_2 treated at 950°C for 5 h) by heating weighed quantities of the mixed components in evacuated silica tubes for 3 days at 800°C. The sintered powders were ground and reannealed at 950°C for 4 days and finally quenched in water without shattering the enclosing silica tubes. Most of the alloys were also subjected to further heat treatments at 500, 650, 800, and 950°C, followed by quenching in water. In order to avoid reactions between the alloys and SiO_2 the samples were placed in crucibles of pure alumina inside the silica tubes. 51 alloys, with nominal composition between 35 and 90 atomic % Mn, were prepared and examined, but only the results for 30 alloys in the range from 44 to 72 atomic % Mn are considered in this paper. Chemical analyses confirmed the composition of 5 representative alloys.

X-Ray powder photographs of all alloys were taken in a Guinier type camera of 80 mm diameter with monochromatized Cu$K\alpha_1$-radiation ($\lambda = 1.54050$ Å) using KCl ($a = 6.2919$ Å [13]) as internal standard. High-temperature X-ray powder photographs were taken in a 190 mm diameter Unicam camera, the samples being sealed in thin-walled quartz capillaries. A 60 mm diameter Debye-Scherrer type camera with asymmetric film mounting was used to collect X-ray data below room temperature. The camera was immersed in liquid helium or liquid nitrogen during the exposures. Filtered Cu$K\alpha$-radiation was used for all X-ray powder photographs taken above or below room temperature.

The lattice dimensions at room temperature were deduced by applying the method of least squares to the diffraction data, and twice the standard deviations obtained in these calculations were taken as error limits. For data collected above or below room temperature, the lattice dimensions were determined from the high-angle reflections, utilizing the Nelson-Riley [14] type extrapolation. For the calculation of X-ray F_c^2-

values, the atomic scattering factors were taken from *International Tables*.[15] The integrated X-ray intensities were measured photometrically.

Powder neutron diffraction data were collected at temperatures between 80 and 425 K, using cylindrical sample holders of aluminium or vanadium. A chromel-alumel thermocouple was inserted inside the sample holder to measure the temperature which was kept constant to within ± 2°C during each experiment. Neutrons of wavelength 1.186 or 1.863 Å were obtained from the reactor JEEP II. Due to the relatively high absorption cross-section of rhodium [15] for thermal neutrons a rectangular sample holder, 3 mm thick, of thin-walled aluminium was used to assemble additional data at room temperature. The use of a flat sample holder was found to give appreciable improvement in intensity and resolution over a cylindrical one. The transmission through the flat samples was determined to be $\exp(-\mu t) = 0.28$.

The integrated intensities were corrected for absorption and converted to jF_o^2 by multiplication with L^{-1}. For the calculation of neutron F_c^2-values, the nuclear scattering lengths ($b_{Rh} = 0.59 \times 10^{-12}$ cm and $b_{Mn} = -0.36 \times 10^{-12}$ cm) were taken from the table published by *The Neutron Diffraction Commission*,[16] and the magnetic form factor for Mn^{2+} from Hastings *et al.*[17]

Magnetic susceptibilities of the alloys were measured between 80 and 1000 K by the Faraday method (maximum field ~ 8000 Ø) using $20-50$ mg samples.

The density measurements were made pycnometrically at 25.00°C with kerosene as displacement liquid. To remove gases adsorbed by the sample (weighing ~ 2 g), the pycnometer was filled with kerosene under vacuum.

RESULTS AND DISCUSSION

(i) *Homogeneity ranges.* Depending on the means of preparation of the samples and the temperature of investigation, we find the cubic and tetragonal RhMn phases in the composition range from 50 to 69 atomic % Mn and the $RhMn_3$ phase above ~ 73 atomic % Mn. The extents of the homogeneity ranges have been determined from the unit cell dimensions (*cf.* Figs. 1, 2), the overall upper and lower limits being also confirmed by application of the disappearing phase principle on the X-ray powder data. Uncertainty attached to some of the phase limits given below, results from the fact that the relatively low transformation temperature between the cubic and tetragonal RhMn phases (*vide infra*) makes it difficult to ascertain whether true thermodynamic equilibrium has been obtained. However, considerable attention was paid to this problem and the internal consistency of the various sets of data indicates that the attempts have been successful.

The homogeneity range of the cubic RhMn phase extends from 50.0 ± 0.5 to ~ 58 atomic % Mn for alloys quenched from temperatures between 500 and 950°C, whereas the tetragonal RhMn phase was found to be homogeneous between ~ 53 and 68.0 ± 0.5 atomic % Mn in the (partly metastable, *vide infra*) room temperature region. Our observation that the tetragonal RhMn phase does not extend to the equiatomic composition at room temperature appears to be consistent with the results of Nakayama and Asanuma [4] and Kasper.[5]

Samples of Rh – Mn alloys in the composition range from ~ 53 to ~ 58 atomic % Mn air cooled to room temperature invariably contained both the cubic and tetragonal RhMn phases (the latter amounting to some 5 % only in alloys with 50 to 55 atomic % Mn). The pure cubic RhMn phase could be obtained by rapidly quenching into iced water relatively small amounts of the alloys containing $50-58$ atomic % Mn sealed in thin-walled quartz tubes

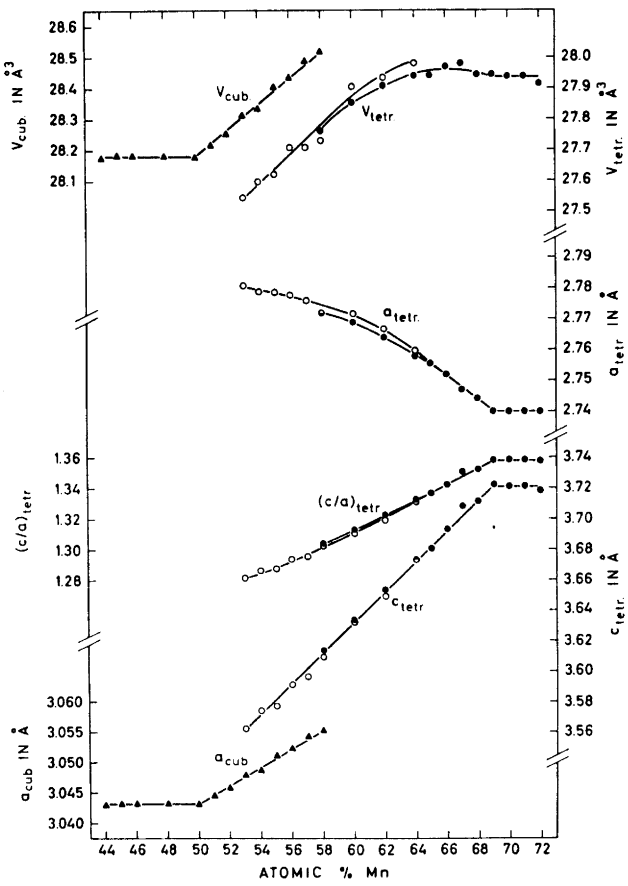

Fig. 1. Unit cell dimensions *versus* composition for the cubic and tetragonal RhMn phases at room temperature. Filled symbols represent samples quenched from $\geqq 500$°C, open circles denote values obtained for samples cycled from room temperature through liquid nitrogen temperature and back to room temperature (see text). The estimated inaccuracies of the parameters do not exceed the size of the symbols.

with internal diameter $\leqq 3$ mm. Most attempts to produce larger quantities of this phase led to mixtures of the cubic and tetragonal RhMn phases, the proportions of the latter increasing with increasing Mn concentration. Alloys containing more than ~58 atomic % Mn gave the pure tetragonal RhMn phase when slowly cooled to room temperature.

The homogeneity range of tetragonal RhMn is appreciably temperature dependent (*cf.* Figs. 1 and 2), the phase limits being determined as 50 ± 1 and 64.0 ± 0.5 atomic % Mn at liquid helium and liquid nitrogen temperatures. Although essential crystallographic details concerning the transformation mechanism between the cubic and tetragonal RhMn phases are lacking, the

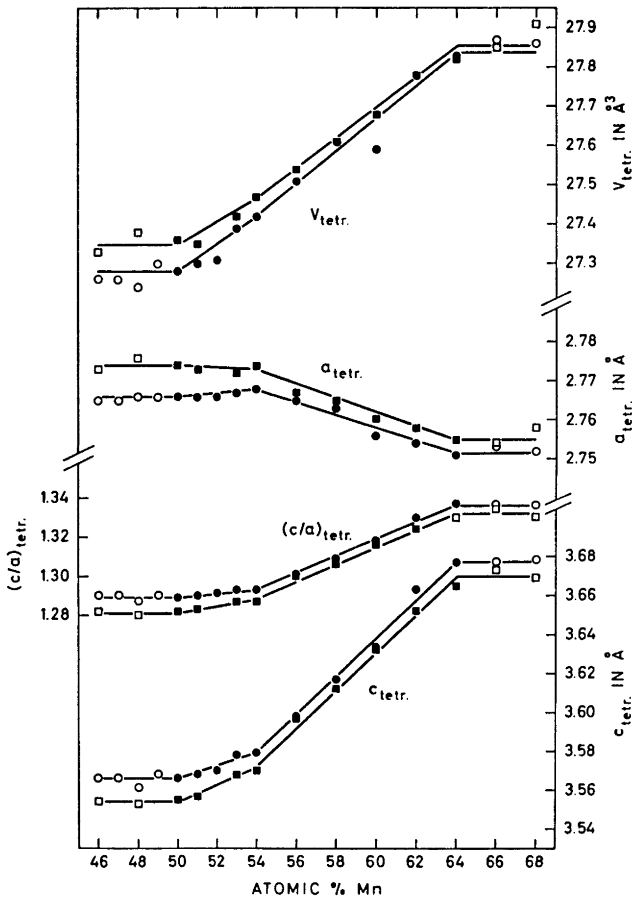

Fig. 2. Variation in lattice parameters of the tetragonal RhMn phase as a function of composition at liquid helium (●) and liquid nitrogen (■) temperatures. Open symbols represent two-phase alloys.

available data (see Refs. 1 – 5 and sections i – iv) suggest very strongly that the transformation may be classified as martensitic (*cf.*, *e.g.*, Ref. 18).

(ii) *Chemical structures.* The solid solutions of the cubic and tetragonal RhMn phases are of the strictly substitutional type, as shown by the comparisons (Fig. 3) of pycnometrically determined densities with those calculated from the unit cell dimensions in Fig. 1.

Comparisons of observed and calculated X-ray intensities confirmed both the CsCl and CuAu(I) type crystal structures (Fig. 4) with less than 10 % primary disorder; and the absence of superstructure reflections gave no evidence of secondary order on the (Rh,Mn) sites in either solid solution. The indicated 10 % limit is imposed by the probable errors in the measurements of the

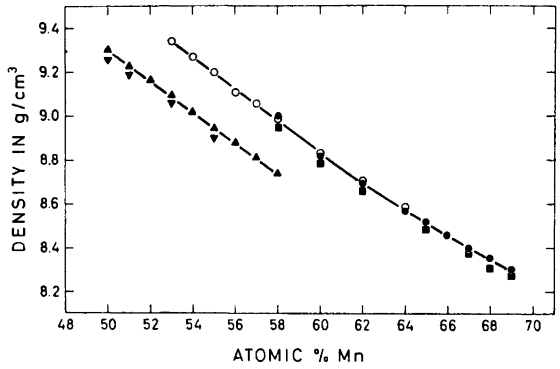

Fig. 3. Compositional dependences of the observed densities of the cubic (▼) and tetragonal (■) RhMn phases compared with those calculated from the unit cell dimensions in Fig. 1 on the basis of substitutional solid solution (▲, ●, ○).

X-ray intensities. The actual value for this parameter is, in fact, almost certainly much lower throughout both solid solution ranges, as evidenced by the neutron diffraction data for four representative alloys (cubic $Rh_{45}Mn_{55}$ and tetragonal $Rh_{45}Mn_{55}$, $Rh_{40}Mn_{60}$, and $Rh_{35}Mn_{65}$) which confirm that the primary disorder does not exceed 3 %.

The shortest interatomic Rh–Mn distances in the cubic RhMn phase at room temperature vary from 2.635 Å at 50 atomic % Mn to 2.646 Å at 58

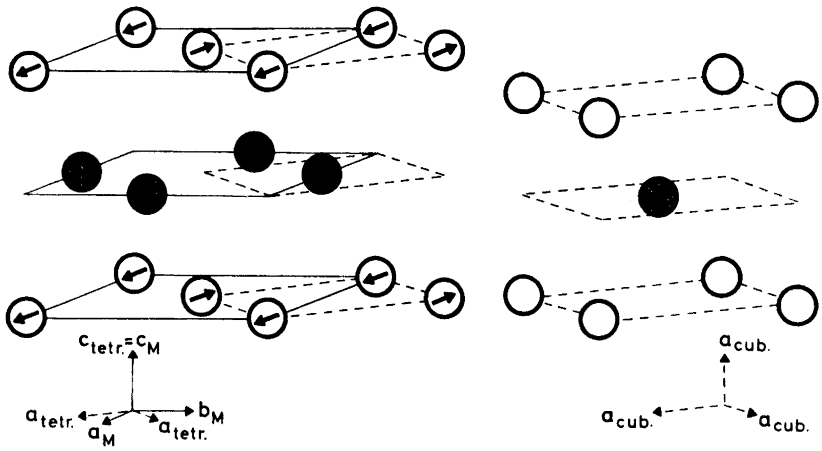

Fig. 4. The chemical and magnetic structures of the tetragonal and cubic RhMn phases. Open circles represent Mn atoms and shaded circles Rh atoms. Magnetic and chemical unit cells are shown by full and broken lines, respectively. The direction of the moments (indicated by arrows) within the (001) planes is undetermined.

atomic % Mn, and are thus very nearly equal to (and show the same trend as) those found for the tetragonal RhMn phase (2.653, 2.666, and 2.686 Å at 53 (metastable at room temperature), 58, and 69 atomic % Mn), which in turn almost match those in the $RhMn_3$ phase (2.694 Å at ~73 atomic % Mn). Together with the atomic volumes, these show a much smaller variation with composition than expected. A linear thermal expansion coefficient of about 1.3×10^{-5} °C^{-1} was obtained for three different alloys of the cubic RhMn phase, thus confirming that this result does not depend on the particular temperature at which they were studied.

The size of the Mn atom is very dependent on its electronic state. Thus Mn, which contributes only two electrons to the conduction band, as in the cubic PdMn phase [11] where it has a spin moment of $2S = 5$, is much larger than in elemental Mn or Mn generally in transition metal alloys. A CN 12 radius of about 1.43 ± 0.02 Å estimated for cubic PdMn is in reasonable agreement with that calculated from the Mn^{VI} radius by Teatum *et al.*[19] Mn is thus larger than Pd in the cubic PdMn phase and this corresponds with the increasing lattice parameter (and hence Pd – Mn distance) on increasing the Mn content.[11] The loss of spin moment with Mn substitution above 50 atomic %, and the corresponding decrease in Mn size, is at a relatively slow rate and does not present difficulties here. In the cubic RhMn phase, however, the spin moment of the alloys falls from $2S \approx 4$ at 50 atomic % Mn to $2S \approx 2$ at 58 atomic % Mn, and assuming that this results from Mn only (which is the case for the tetragonal RhMn phase; see section iii), it should be accompanied by a rapid decrease in the size of Mn from ~1.35 to ~1.29 Å (for CN 12 and ~3 and ~4 bonding electrons per Mn atom, respectively). These expected changes of size are certainly not reflected in the variation of the interatomic Rh – Mn distances, which show a linear *increase* between 50 and 58 atomic % Mn (*vide supra*).

In the tetragonal RhMn phase the variation of the unit cell dimensions with composition (Fig. 1) is in accordance with those already found and discussed for the isostructural phases of Mn and Ir, Ni, Pd, or Pt,[6–8,11] namely that $c_{tetr.}$ decreases and $a_{tetr.}$ increases on moving towards the equiatomic composition.

A dominant feature of Fig. 2 is the discontinuities in the slopes at 54 atomic % Mn of the unit cell dimensions *versus* composition curves for the single phase region of tetragonal RhMn. In particular, the values of $a_{tetr.}$ in the range 50 – 54 atomic % Mn are substantially constant. This effect is probably due to magnetostriction owing to a smaller separation from the Néel point at the temperatures of observation, for alloys in the latter composition region. Magnetostriction is also apparent in the observed transposed relationship between the data obtained for $a_{tetr.}$ and $c_{tetr.}$ at liquid helium and liquid nitrogen temperatures. This behaviour appears to be analogous with that noted earlier in the thermal expansion curves for alloys of the isostructural PdMn phase.[11]

(iii) *Magnetic structures.* The neutron diffraction pattern of cubic $Rh_{45}Mn_{55}$ at room temperature definitely shows no purely magnetic reflections, and any contribution of magnetic origin to the nuclear reflections must be small. A small magnetic contribution to the nuclear peaks is hard to detect, but from

Table 1. Comparison of observed and calculated neutron diffraction data.

Phase T(K)		Tetr. $Rh_{45}Mn_{55}$[a] 80		Tetr. $Rh_{40}Mn_{60}$ 80		Tetr. $Rh_{40}Mn_{60}$ 293		Tetr. $Rh_{35}Mn_{65}$ 293	
hkl	Type	jF_o^2	jF_c^2	jF_o^2	jF_c^2	jF_o^2	jF_c^2	jF_o^2	jF_c^2
100	Magn	4.34	4.40	4.73	4.74	4.63	4.72	4.12	4.21
001	Nucl	5.62	5.92	4.29	4.72	4.71	4.72	3.63	3.59
110	Nucl	11.92	11.84	9.96	9.44	9.50	9.44	7.46	7.18
101	Magn	8.87	8.72	9.91	9.92	10.16	9.89	8.64	8.77
111	Nucl	0	0.64	0	0.08	0	0.08	0	0.08
200	Nucl	0	0.32	0	0.04	0	0.04	0	0.04
002	Nucl	0	0.16	0	0.02	0	0.02	0	0.02
210	Magn	2.01	1.94	22.33	{ 2.18	21.56	{ 2.17	16.98	{ 1.94
201	Nucl	24.93	23.68		{18.88		{18.88		{14.36
102	Magn	2.31	3.10	3.85	3.34	3.60	3.33	3.08	2.97
211	Magn	3.00	3.46	3.39	3.73	3.65	3.71	3.64	3.28
112	Nucl	22.08	23.68	17.24	18.88	17.48	18.88	14.04	14.36
220	Nucl			0	0.04	0	0.04	0	0.04
202	Nucl			0	0.08	0	0.08	0	0.08
300	Magn			19.40	{ 0.33	19.63	{ 0.33	13.83	{ 0.28
221	Nucl				{18.88		{18.88		{14.36
R		0.056		0.052		0.033		0.037	

[a] Cubic $Rh_{45}Mn_{55}$; $T=293$ K; $h^2+k^2+l^2$, jF_o^2, jF_c^2; 1, 4.99, 4.48; 2, 0.28, 0.25; 3, 6.01, 5.97; 4, 0, 0.13; 5, 17.37, 17.92; $R=0.039$.

the agreement between jF_o^2 and jF_c^2 shown in Table 1 we estimate the maximum value for any possible ordered moment to be 0.1 B.M. The lack of cooperative magnetism for the cubic RhMn phase is consistent with previous findings for the isostructural NiMn[20–22] and PdMn[11,21] phases.

The neutron diffraction patterns of tetragonal $Rh_{45}Mn_{55}$, $Rh_{40}Mn_{60}$, and $Rh_{35}Mn_{65}$ (Table 1) were indexed in terms of C-centred cells with $a_M=\sqrt{2}a_{tetr.}$ and $c_M=c_{tetr.}$ (Fig. 4). Reflections with $h+k=2n$ are purely nuclear and those with $h+k=2n+1$ are purely magnetic, corresponding to antiferromagnetic alignment of moments related *via* the C-centres. The magnetic structures of the three alloys are of orthorhombic or lower symmetry and the directions of the moments are perpendicular to [001]. The deduced spin quantum numbers amount to $2S_{Mn}=3.4\pm0.2$ for $Rh_{45}Mn_{55}$ and $Rh_{40}Mn_{60}$ whereas $2S_{Mn}=3.2\pm0.2$ was found for $Rh_{35}Mn_{65}$. Within the experimental accuracy, the Rh atoms were found to be non-magnetic, *i.e.* $2S_{Rh}<0.2$. These results agree well with those of a corresponding study on tetragonal $Rh_{50}Mn_{50}$ by Kasper,[5] who found the same type of antiferromagnetic order at 77 K with $2S_{Mn}\approx3.3$ and $2S_{Rh}\approx0.0$.

The directions of the moments within the (001) planes are inaccessible on the basis of neutron powder diffraction data. Using the Landau theory for second-order transformations Krén and Sólyom[23] deduce that only two possible directions of the moments, *i.e.* [100] and [110] and equivalent directions of the magnetic cell (Fig. 4), can arise from a single second-order transition

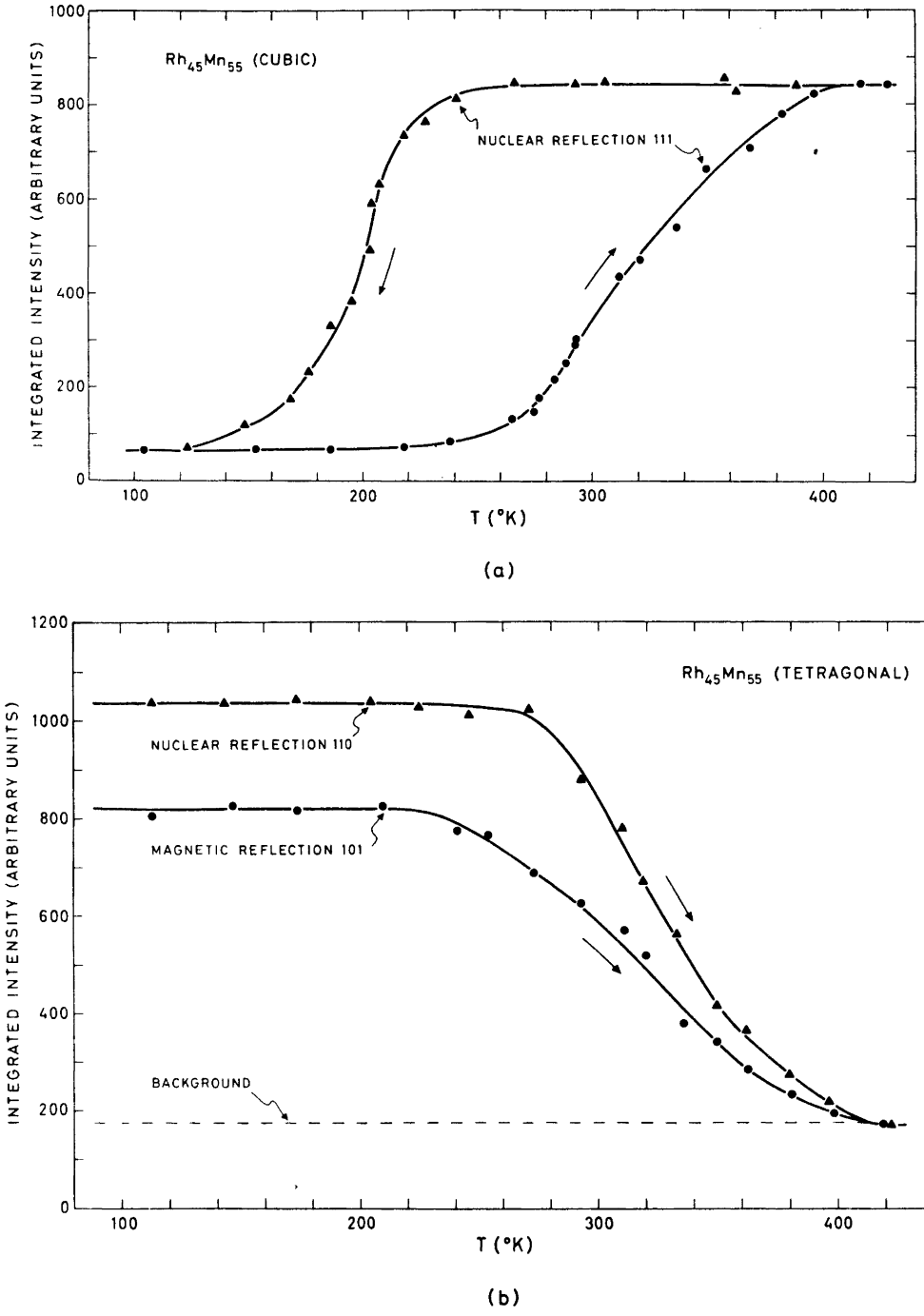

Fig. 5. Temperature dependence of the integrated intensity of (a) the nuclear reflection 111 of cubic $Rh_{45}Mn_{55}$ and (b) the nuclear reflection 110 and the magnetic reflection 101 of tetragonal $Rh_{45}Mn_{55}$.

between a paramagnetic and an antiferromagnetic state. This requirement is not satisfied in the present case, as is clearly demonstrated by the temperature variations of characteristic nuclear and magnetic reflections for cubic and tetragonal $Rh_{45}Mn_{55}$ (Fig. 5a, b). In particular, the simultaneous disappearance and virtually parallel behaviour of the nuclear reflection 110 and the magnetic reflection 101 of tetragonal $Rh_{45}Mn_{55}$ on heating and the fact that the latter curve does not follow a Brillouin type function (Fig. 5b), demonstrate that we have no single second-order transition. No limitation can accordingly be set on the direction of the moments within (001). Neglecting this uncertainty, the antiferromagnetic ordering of the first kind in the tetragonal RhMn phase matches that found for the chemically isostructural IrMn,[12] NiMn,[20-22,24] and PdMn [11,21,23,25] phases and also for the PtMn [9,10,21,26,27] phase depending on composition and temperature.

(iv) *Magnetic susceptibility.* Magnetic susceptibility data were collected for all samples in the range 46 – 65 atomic % Mn, and the results show a systematic variation with composition. In order to avoid confusion, only the thermomagnetic data for four representative alloys are reproduced in Fig. 6. The curves have the following characteristics:

The cooling curves consist of two distinct linear sections, which can be described by Curie-Weiss Law relationships, *viz.* $\chi^{-1} = C^{-1}(T - \Theta)$. A phase transition between two paramagnetic phases is indicated at the intercept, T_{trans}, between the two sections. A

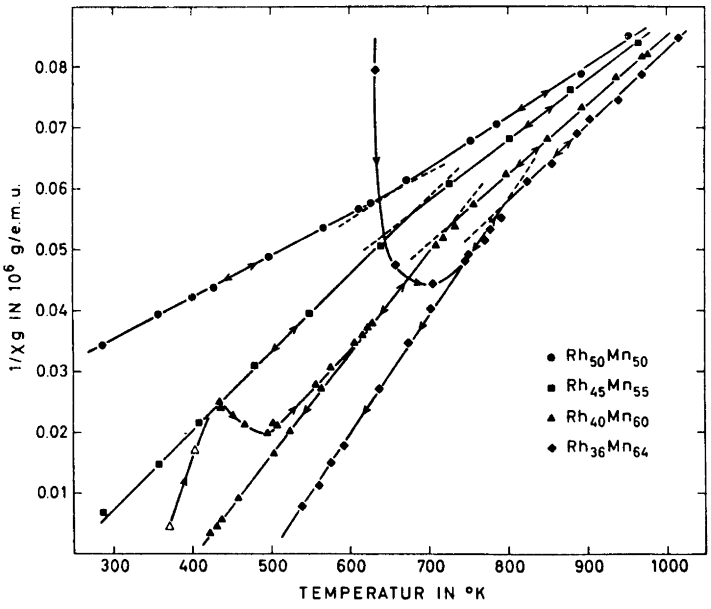

Fig. 6. Temperature dependence of the reciprocal magnetic susceptibility above room temperature for four representative alloys in the equiatomic region of the Rh–Mn system. The arrrows indicate the direction of temperature change, and open symbols represent field strength dependent susceptibilities.

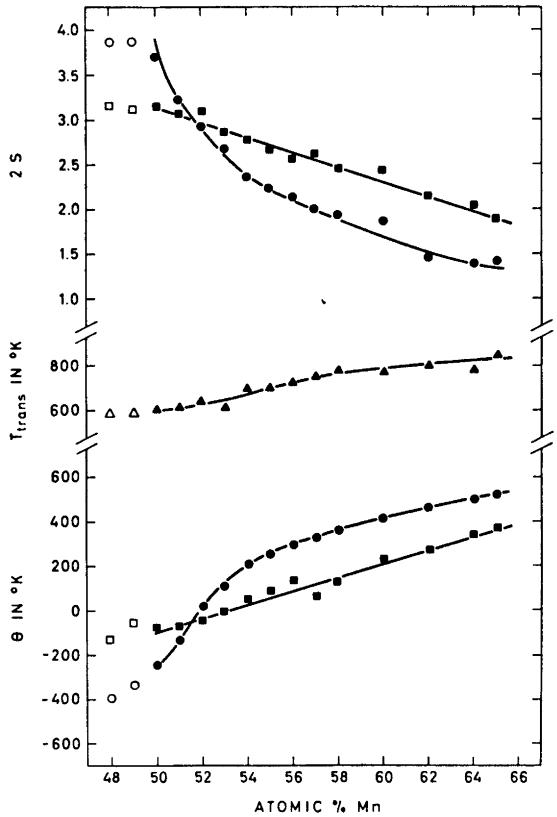

Fig. 7. $2S_{Mn}$, θ, and $T_{trans.}$ for the ordered and disordered cubic RhMn phases as a function of Mn content. ●, data for the ordered phase; ■, data for the disordered phase; ▲, $T_{trans.}$ Open symbols indicate two-phase samples.

gradual change of slope such as reported by Nakayama and Asanuma [4] was not observed. The compositional dependence of the transition temperatures, lying between 580 and 840 K, is given in Fig. 7. The θ values of the two sections of the curves, and the spin quantum numbers $2S_{Mn}$ (neglecting the possibility of a small moment associated with the Rh-atoms (see section iii)) calculated on the "spin only" approximation, $\mu = \sqrt{8C}_{mol} = 2\sqrt{S(S+1)}$, are also included in Fig. 7. The rapid decrease of $2S_{Mn}$ with increasing Mn content above 50 atomic % for both low and high temperature paramagnetic states is noteworthy. So also is the increasing value of the parameter θ as the Mn content of the alloys increases.

The heating curves are found to lie above the cooling curves at lower temperatures, and a peak is observed in the $\chi^{-1}(T)$-curves above room temperature for samples with > 54 atomic % Mn heated from liquid nitrogen temperature (or > 58 atomic % Mn heated from room temperature; *cf.* Fig. 6). For temperatures below those corresponding to the maximum in χ^{-1}, the susceptibilities are field strength dependent. The maximum values of χ^{-1} depend rather critically on the low temperature treatment of the samples, whereas the temperatures at which the maxima occur are relatively independent of this treatment. The heating curves coincide with the cooling curves before $T_{trans.}$ is reached.

A comparison of the magnetic susceptibility and X-ray data shows that the linear parts of the $\chi^{-1}(T)$-curves correspond to paramagnetic states of cubic RhMn, and the non-linear part to the antiferromagnetic state of the tetragonal RhMn phase. A possible cause of the abrupt change of moment at $T_{trans.}$ for cubic RhMn is a transformation from an ordered to an essentially disordered chemical structure. This interpretation appears to be consistent with the high temperature X-ray data and is in agreement with similar findings for the NiMn phase.[20,22]

No evidence for the weak ferromagnetism observed in the magnetic susceptibility measurements has been detected in the neutron diffraction data of tetragonal RhMn. Thus, it may be attributed to a small canting of the antiferromagnetically aligned moments in the tetragonal phase, which cannot be detected with the available neutron diffraction technique; or to the presence of traces of ferromagnetic impurities. Considering all available data, we prefer the first explanation.

The size of the spin quantum number for tetragonal RhMn as determined by neutron diffraction can, broadly speaking, be explained by the model previously proposed to account for the spin moments in tetragonal NiMn, PdMn, and PtMn.[9–11] In these phases there is an average of approximately one s electron per atom in the conduction band, five d electrons on Mn and approximately ten d electrons on the other metal atom. The ligands split the degeneracy of the Mn d orbitals, but the splitting is insufficient to prevent Mn from assuming a "high-spin" state with one electron in each of the d_{xy}, d_{yz}, d_{zx}, $d_{x^2-y^2}$ and d_{z^2} orbitals. If we orient d_{xy} to point along $[\pm 100]$ and $[0\pm 10]$ of the chemical unit cell, d_{yz} and d_{zx} point along $[\pm 1\pm 1\pm 1]$ in the cubic cell, and close to this in the tetragonal. Similarly $d_{x^2-y^2}$ is directed along $[\pm 1\pm 10]$ and d_{z^2} along $[00\pm 1]$. The critical Mn – Mn separation for a transition from localized to interacting non-localized d electrons is ~ 3.0 Å.

In tetragonal RhMn the d_{xy} electrons of Mn overlap with those of its four neighbours at ~ 2.75 Å in the (001) plane to form a bonding energy band, so reducing the number of unpaired electrons on Mn from five to four. The further reduction from 4.0 to ~ 3.4 unpaired electrons observed for $Rh_{50}Mn_{50}$ presumably reflects the lowering of the Fermi level resulting from Rh having one valence electron less than Ni, Pd, and Pt.

The model implies that the interlayer Mn – Mn contacts in alloys with > 50 atomic % Mn should reduce the number of unpaired electrons per Mn atom at a rate of $2S = 0.04$ per atomic % Mn (by the pairing of two electrons in d_{yz} and d_{zx} orbitals which are directed from the Mn atoms to the metal atoms in neighbouring layers). The results given in section iii suggest that this simple chemical bond scheme may be essentially correct.

By assuming that Mn – Mn interatomic distances > 3.04 Å exceed the critical distance for the occurrence of non-localized d electrons, the observation of ~ 4 unpaired electrons per Mn atom in chemically ordered cubic $Rh_{50}Mn_{50}$ is readily explained by the model (corresponding to the observation of 5 unpaired electrons in cubic PdMn [11]).

The strong reduction in $2S_{Mn}$ with increasing Mn content in the region of cubic RhMn, where the ordered CsCl type structure prevails, indicates that each Mn substituted for Rh initially eliminates the entire $2S \approx 4$ spin moments

on its 8 Mn nearest neighbours, by creating a band overlap, so that the Mn spin moment decreases at a rate of $2S \approx 0.32$ per atomic % Mn substituted above 50 %. Thus, as observed in Fig. 7, at about 56 atomic % Mn the spin moment is reduced from ~ 4 to ~ 2, and there is a major breakdown of the simple electron pairing model. Thereafter the rate of disappearance of Mn spin moment decreases greatly, and is probably not significantly different from that found for the high-temperature paramagnetic phase.

The magnetic susceptibility data of the high-temperature cubic RhMn phase is another indication that this phase is essentially disordered. Thus, the spin moment of Mn in high-temperature $Rh_{50}Mn_{50}$ is lower, and the spin moments decrease less rapidly with increasing Mn content than in the ordered phase with CsCl type structure.

Lacking magnetic susceptibility data at and above T_N for the tetragonal RhMn, it is impossible to carry out a detailed analysis of the exchange interactions in this phase.

For cubic RhMn the gradual changes in the $\chi^{-1}(T)$ curves (Fig. 6), and in particular the change in size of θ with composition, suggest that at least two different exchange mechanisms are operative. Since $\sum_i z_i J_i/k = 3\theta/2S(S+1)$* changes from -71 to 341 K between 50 and 60 atomic % Mn (from the low temperature Curie-Weiss relationships; *cf.* Fig. 7), a ferromagnetic type of coupling appears to dominate in the Mn-rich alloys, and antiferromagnetic coupling in the Mn-poor. (It must be emphasized, however, that the cubic RhMn phase has not been obtained in an ordered magnetic state.) The "exchange parameters" $\sum_i z_i J_i/k$ (-29 to $+125$ K between 50 and 60 atomic % Mn) deduced from the high temperature Curie-Weiss relationships are generally smaller than those established from the corresponding low temperature relationships. The abrupt decrease in $\sum_i z_i J_i/k$ at $T_{\text{trans.}}$ on increasing the temperature can occur in several ways; *e.g.* the J_i values may decrease numerically (including some of them to be zero), the z_i's may become smaller, relative changes may occur in the z_i's, or the sign of some of the J_i terms may change. A combination of several of these factors is quite probable, *i.e.* consistent with the "critical distance" interpretation given above. Lack of data prevents further resolution of the parameters z_i and J_i.

REFERENCES

1. Hansen, M. (and Anderko, K.) *Constitution of Binary Alloys*, McGraw, New York – Toronto – London 1958, p. 948.
2. Raub, E. and Mahler, W. *Z. Metallk.* **46** (1955) 282.
3. Kouvel, J. S., Hartelius, C. C. and Osika, L. M. *J. Appl. Phys.* **34** (1963) 1095.
4. Nakayama, Y. and Asanuma, M. *J. Appl. Phys. (Japan)* **4** (1965) 315.
5. Kasper, J. S. *Private communication;* see also Kouvel, J. S. In Westbrook, J. H. *Intermetallic Compounds*, Wiley, New York – London – Sydney 1967, Chapter 27.
6. Brun, K., Kjekshus, A. and Pearson, W. B. *Phil. Mag.* **10** (1964) 291.
7. Brun, K., Kjekshus, A. and Pearson, W. B. *Acta Chem. Scand.* **19** (1965) 107.

* J_i is the exchange interaction between the z_i i-th nearest Mn neighbours and k is Boltzmann's constant.

8. Pearson, W. B., Brun, K. and Kjekshus, A. *Acta Chem. Scand.* **19** (1965) 477.
9. Andresen, A. F., Kjekshus, A., Møllerud, R. and Pearson, W. B. *Phil. Mag.* **11** (1965) 1245.
10. Andresen, A. F., Kjekshus, A., Møllerud, R. and Pearson, W. B. *Acta Chem. Scand.* **20** (1966) 2529.
11. Kjekshus, A., Møllerud, R., Andresen, A. F. and Pearson, W. B. *Phil. Mag.* **16** (1967) 1063.
12. Selte, K., Kjekshus, A., Andresen, A. F. and Pearson, W. B. *Acta Chem. Scand.* **22** (1968) 3039.
13. Hambling, P. G. *Acta Cryst.* **6** (1953) 98.
14. Nelson, J. B. and Riley, D. P. *Proc. Phys. Soc.* **57** (1945) 160.
15. *International Tables for X-Ray Crystallography*, Kynoch Press, Birmingham 1962, Vol. III.
16. The Neutron Diffraction Commission, *Acta Cryst.* **A 25** (1969) 391.
17. Hastings, J. M., Elliott, N. and Corliss, L. M. *Phys. Rev.* **115** (1959) 13.
18. Christian, J. W., Read, T. A. and Wayman, C. M. In Westbrook, J. H. *Intermetallic Compounds*, Wiley, New York – London – Sydney 1967, Chapter 22.
19. Teatum, E., Gschneider, K. and Waber, J. *U.S.A.E.C. Research Paper LA-2345* 1960.
20. Krén, E., Nagy, E., Nagy, I., Pál, L. and Szabó, P. *J. Phys. Chem. Solids* **29** (1968) 101.
21. Pál, L., Krén, E., Kádár, G., Szabó, P. and Tarnóczi, T. *J. Appl. Phys.* **39** (1968) 538.
22. Pál, L., Tarnóczi, T. and Konczos, G. *Phys. Status Solidi* **42** (1970) 49.
23. Krén, E. and Sólyom, J. *Phys. Letters* **22** (1966) 273.
24. Kasper, J. S. and Kouvel, J. S. *J. Phys. Chem. Solids* **11** (1959) 231.
25. Gonzalo, J. A. and Kay, M. I. *J. Phys. Soc. Japan* **21** (1966) 1626.
26. Krén, E., Cselik, M., Kádár, G. and Pál, L. *Phys. Letters* **A 24** (1967) 198.
27. Krén, E., Kádár, G., Pál, L., Sólyom, J., Szabó, P. and Tarnóczi, T. *KFKI Report 2*, Hungarian Academy of Sciences, 1968.

Received May 27, 1971.